Colorimetric sensing of iodide based on triazole-acetamide functionalized gold nanoparticles

I-Lin Lee, Yi-Ming Sung, Chien-Hou Wu & Shu-Pao Wu

Microchimica Acta
Analytical Sciences Based on Micro- and Nanomaterials

ISSN 0026-3672
Volume 181
Combined 5-6

Microchim Acta (2014) 181:573-579
DOI 10.1007/s00604-013-1150-0

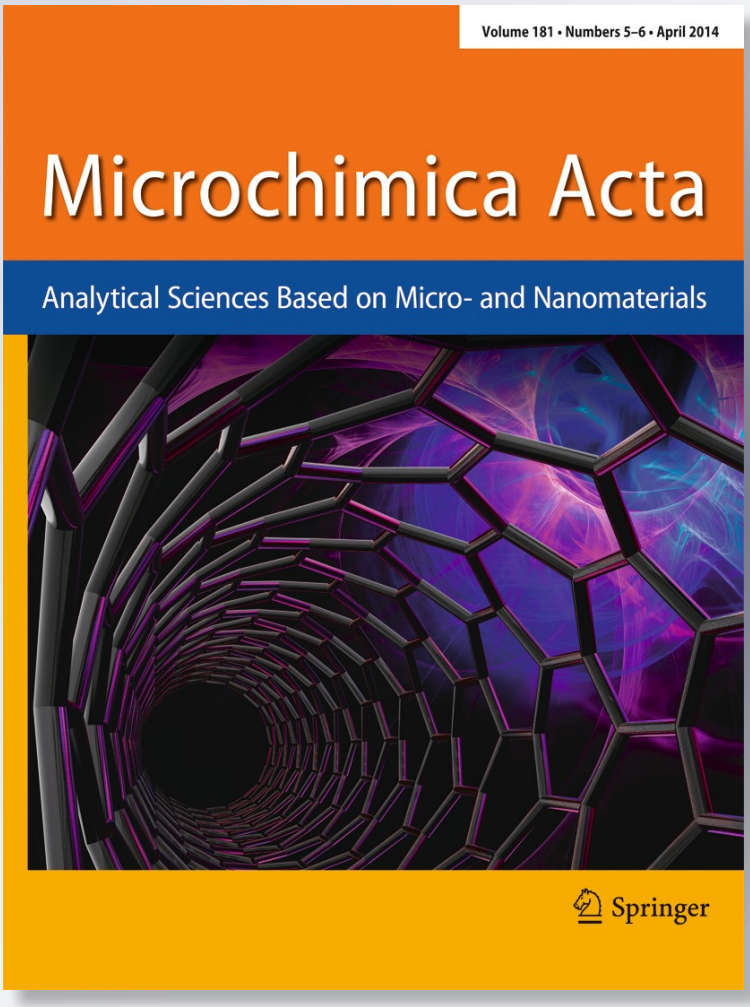

Springer

Microchim Acta (2014) 181:573–579
DOI 10.1007/s00604-013-1150-0

ORIGINAL PAPER

Colorimetric sensing of iodide based on triazole-acetamide functionalized gold nanoparticles

I-Lin Lee · Yi-Ming Sung · Chien-Hou Wu · Shu-Pao Wu

Received: 22 August 2013 / Accepted: 15 December 2013 / Published online: 7 January 2014

Abstract We have modified gold nanoparticles (AuNPs) with triazole acetamide to obtain a material for the sensitive and selective colorimetric determination of iodide. The functionalized AuNPs were prepared by a reductive single chemical step using a Cu(I)-catalyzed click reaction. The presence of iodide ions induces the aggregation of these AuNPs and results in a color change from wine-red to purple. The iodide-induced aggregation can be detected visually with bare eyes, but also by photometry. The detection limit is as low as 15 nM. The method displays excellent selectivity for iodide over other anions due to the selective interaction with the amido groups of the triazole. The method was applied to the determination of iodide in spiked lake waters.

Keywords Colorimetric sensor · Iodide · Gold nanoparticles · Triazole

Introduction

Iodide is known to be an essential nutrient in the human body. In the thyroid gland, iodine is utilized for the biosynthesis of the thyroid hormones thyroxin (T4) and triiodothyronine (T3), which are important in metabolism and mental development [1, 2]. The recommended daily intake of iodide is 150 μg/day. Shortage of iodide can cause a severe interruption in neurological development and can result in diseases such as goiter and hypothyroidism. Conversely, an excess of iodine or iodide ingestion can also cause hyperthyroidism [3].

Several methods for the detection of I^- have been developed, including ion chromatography [4, 5], electrochemistry [6–8], and organic chromophores or fluorophores [9–15]. However, these methods have some limitations, such as long examination time, low precision, and high detection limits. Colorimetric assays based on functionalized gold nanoparticles (AuNPs) can provide an easy way to solve these limitations.

AuNPs show surface plasmon resonance (SPR) absorption properties, which are particularly sensitive to size, shape, and interparticle distance [16, 17]. Many AuNP-based colorimetric sensors use interparticle plasmon coupling for analyte detection [18]. In these assays, analyte-induced aggregation of AuNPs leads to a red shift in the SPR absorption band, resulting in a red-to-blue color change. On the other hand, the removal of analyte results in the redispersion of the aggregated AuNPs, causing the color to revert from blue to red. The distance-dependent SPR absorption of AuNPs has become a useful tool for the development of colorimetric sensing of various analytes, such as metal ions [19–22] and anions [10, 23–25].

In this study, triazole-acetamide functionalized gold nanoparticles (ATTP-AuNPs) were synthesized for detecting I^-. Gold nanoparticles were prepared through borohydride-mediated reduction of $HAuCl_4$. 5-(1,2-Dithiolan-3-yl)-*N*--(prop-2-yn-1-yl)pentanamide (TP) was attached to the surface of AuNPs through the dithiol group. Finally, the azide part of azidoacetamide and the acetylene part of TP were combined to form a triazole structure on the surface of AuNPs through click reaction. The synthesized *N*-{[1-(2-amino-2-oxoethyl)-1H-1,2,3-triazol-4-yl]methyl}-5-(1,2-dithiolan-3-yl) pentanamide AuNPs (ATTP-AuNPs) can be used for anion detection (Scheme 1). Anions such as Br^-, Cl^-, CN^-, ClO_4^-,

Electronic supplementary material The online version of this article (doi:10.1007/s00604-013-1150-0) contains supplementary material, which is available to authorized users.

I.-L. Lee · Y.-M. Sung · S.-P. Wu (✉)
Department of Applied Chemistry, National Chiao Tung University, Hsinchu, Taiwan, Republic of China
e-mail: spwu@mail.nctu.edu.tw

C.-H. Wu
Department of Biomedical Engineering and Environmental Sciences, National Tsing Hua University, Hsinchu, Taiwan, Republic of China

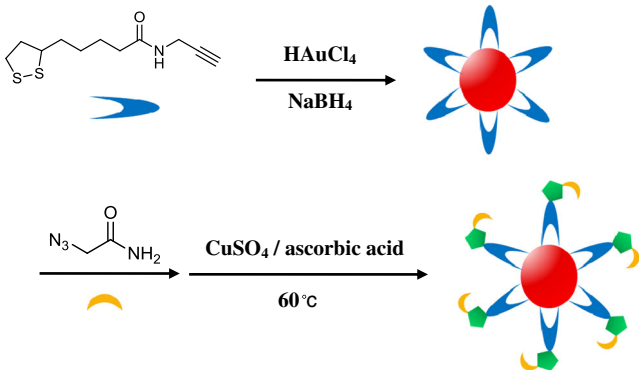

Scheme 1 Synthesis of ATTP-AuNPs

F^-, HSO_4^-, $H_2PO_4^-$, HPO_4^{2-}, I^-, NO_3^-, OAc^-, OH^-, pyrophosphate (PPi), S^{2-}, $S_2O_3^{2-}$, and SCN^- were tested for metal ion selectivity. However, I^- was the only anion that caused the aggregation of ATTP-AuNPs. This caused the SPR absorption band of ATTP-AuNPs to shift to a longer wavelength, and consequently caused a color change from wine-red to purple, which could be used to detect the presence of I^- ions. The SPR absorption at 700 nm directly indicated the degree of ATTP-AuNP aggregation caused by the addition of I^- ions.

Experimental

Chemicals

NaCl, $Na_2S_2O_3{\cdot}5H_2O$, Hydrogen tetrachloroaurate(III) tetrahydrate and $Na_2HPO_4.12H_2O$ were purchased from Showa (www.showa-chemical.co.jp/english/index.html). Lipoic acid, N,N-diisopropylethylamine were purchased from Acros (www.acros.com/). Propargylamine, *O*-(benzotriazol-1-yl)-*N*,*N*,*N*′,*N*′-tetramethyluroniumhexafluoro phosphate (HBTU), 2-bromoacetamide, L-ascorbic acid sodium salt, NaI were purchased from Alfa Aesar (www.alfa.com/). Sodium borohydride, sodium azide, copper sulfate, $[CH_3(CH_2)_3]_4N(OH)$, $[CH_3(CH_2)_3]_4NBr$, $[CH_3(CH_2)_3]_4N(CN)$, $[CH_3(CH_2)_3]_4NF.\chi H_2O$, $[CH_3(CH_2)_3]_4N(HSO_4)$, $[CH_3(CH_2)_3]_4NI$, $[CH_3(CH_2)_3]_4N(NO_3)$, $[CH_3(CH_2)_3]_4N(OAc)$, $[CH_3(CH_2)_3]_4N(SCN)$, $Na_2S{\cdot}9H_2O$ and KBr were purchased from Sigma-Aldrich (www.sigmaaldrich.com/taiwan.html). $Na_4P_2O_7$ was purchased from Riedel-de Haen. $[CH_3(CH_2)_3]_4N(H_2PO_4)$ was purchased from J.T. Baker (www.avantormaterials.com/). $[CH_3(CH_2)_3]_4N(ClO_4)$ was purchased from TCI (www.tcichemicals.com/en/tw/index.html). For all aqueous solutions, deionized water (resistivity, 18.0 MΩ.cm at 25 °C) purified by Millipore Direct-Q water purification unit was used.

Instruments

Absorption spectra were measured on an Agilent 8453 UV-vis spectrometer (Santa Clara, CA, USA) using a 1.0 cm quartz cell. IR spectra were recorded with KBr pellets on Bomem DA8.3 FTIR spectrometer (Quebec, Canada). HR-TEM images were obtained from JEOL JEM-3000F high-resolution transmission electron microscope (Tokyo, Japan). The average size of nanoparticles was statistically determined by measuring the diameter of 150 particles from the HR-TEM image using ImageJ software. The size distribution of ATTP-AuNPs was also characterized by dynamic light scattering (Nano-ZS ZEN3600, Malvern Instruments, Germany). ICP-MS data were acquired on ICP-MS Perkin Elmer, SCIEX ELAN 5000 (Waltham, MA, USA).

Synthesis of ATTP-AuNPs

5-(1,2-Dithiolan-3-yl)-*N*-(prop-2-yn-1-yl)pentanamide (TP) and azidoacetamide were synthesized as references [26, 27]. Gold nanoparticles were prepared by reducing $HAuCl_4$ with sodium borohydride. All glassware was thoroughly cleaned with aqua regia (3:1 HCl/HNO_3) and rinsed with deionized water prior to use. Briefly, To 100 mL deionized water, $HAuCl_4$ (80 mM, 270 μL) and TP (10 mM, 50 μL) were added and stirred for 15 min. Freshly prepared sodium borohydride (0.1 M, 1 mL) was added dropwise to the mixture and stirred for 2 h. The color of the aqueous solution became wine-red, indicating that TP-capped gold nanoparticles formed. Then azidoacetamide (10 mM, 50 μL) was added to the TP-AuNPs solution. The

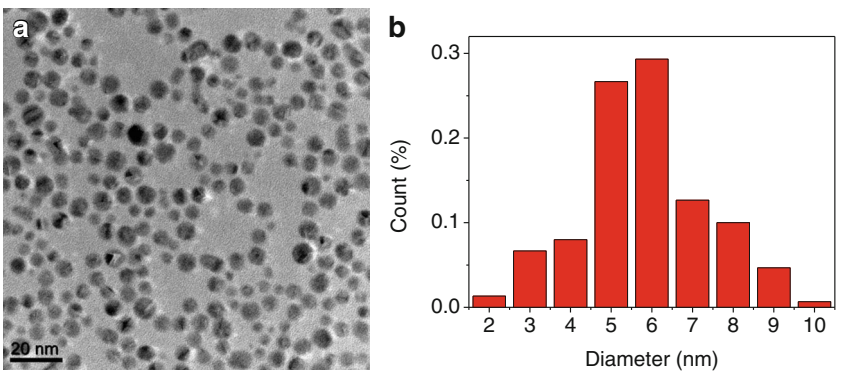

Fig. 1 **a** TEM image of ATTP-AuNPs. The scale bar is 20 nm. **b** The size distribution of ATTP-AuNPs. The total number of the counted particles in the TEM image is 150

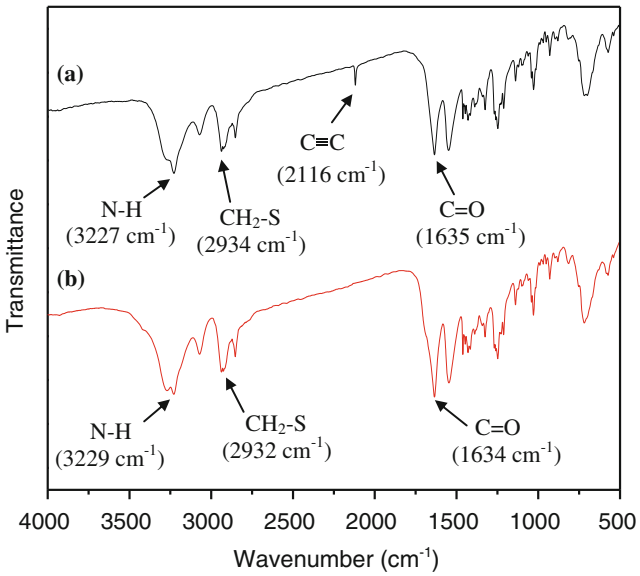

Fig. 2 FT-IR spectra of **a** TP-AuNPs and **b** ATTP-AuNPs

mixture was stirred for 15 min, and heated to 60 °C. To this mixture, a solution of sodium ascorbate (20 mM, 100 μL) mixed with copper sulfate (2 mM, 100 μL) was added slowly and stirred for a further 2 h. After cooled to room temperature, ATTP-AuNPs were purified by dialysis membrane (Spectra/Pro7 Membrane, MWCO 3500) for 3 h, with three changes of the deionized water (at 1 h interval), to remove impurities.

Colorimetric detection of I^- ions

To a 1.0 mL of solution containing ATTP-AuNPs, different anions (5 μM) were added separately. The mixture were maintained at room temperature for 10 min and then transferred separately into a 1.0 cm quartz cell. The absorption spectra were recorded by UV-vis spectrometer.

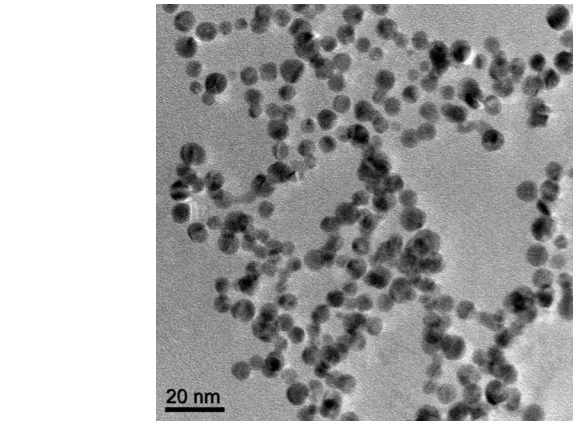

Fig. 4 TEM image of ATTP-AuNPs in the presence of I^- (5 μM)

Analysis of lake water samples

Water samples from the lake located in NCTU, Hsinchu, Taiwan, were collected and filtered through a 0.2 μm membrane. To the 500 μL of lake water, different volumes (20, 40, and 50 μL) of I^- standard solution (100 μM) were spiked separately. The spiked samples were then added to the 500 μL of ATTP-AuNPs solutions and maintained at room temperature for 10 min. The final concentrations of I^- were 2.0, 4.0, and 5.0 μM, respectively. The analytical results were obtained by ICP-MS and the developed sensing method.

Results and discussion

Characterization of ATTP-AuNPs

Gold nanoparticles were prepared through the borohydride-mediated reduction of $HAuCl_4$. 5-(1,2-Dithiolan-3-yl)-

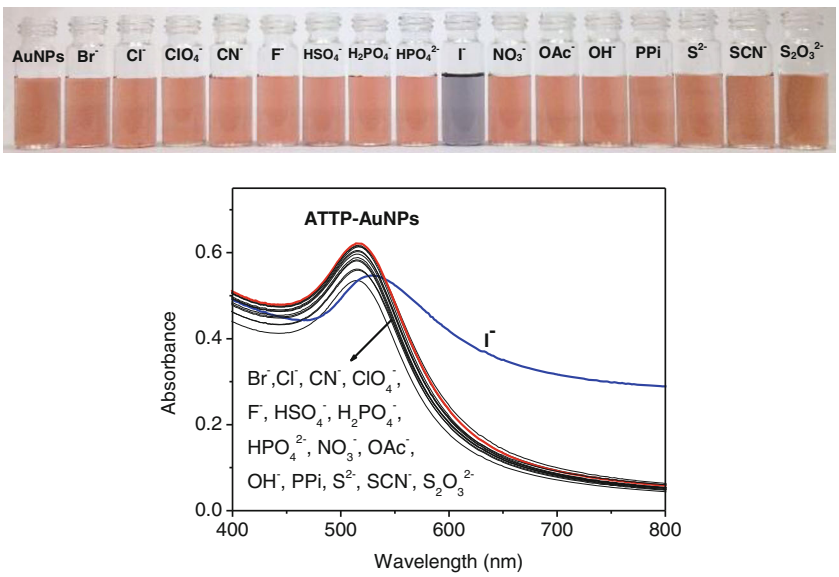

Fig. 3 UV–vis spectra of ATTP-AuNPs in the presence of various anions (4 μM)

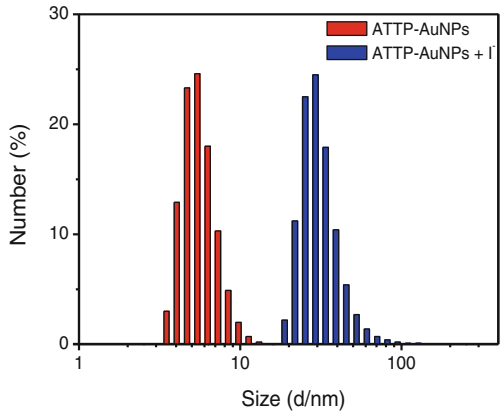

Fig. 5 Size distribution of ATTP-AuNPs (*red bar*) and ATTP-AuNPs with iodide ions (*blue bar*) measured by dynamic laser scattering (DLS)

N-(prop-2-yn-1-yl)pentanamide (TP) was added to the AuNP solution to be used as the capping agent. The azide part of azidoacetamide and the acetylene part of TP were combined to form a triazole structure under the click reaction. The synthesized ATTP-AuNPs could be used for further studies (Scheme 1). Transmission electron microscopy (TEM) images reveal that the particle sizes of ATTP-AuNPs ranged from 2 nm to 10 nm, and most particle sizes fell in the range of 5–6 nm (Fig. 1). The cycloaddition products from the click reaction were verified by infrared spectroscopy. As shown in Fig. 2a, the characteristic skeleton peaks of TP-AuNPs are at 3,227 cm^{-1} (N-H), 2,934 cm^{-1} (CH_2-S), and 2,116 cm^{-1} (–C≡CH). In Fig. 2b, the peak that was originally at 2,116 cm^{-1} (–C≡CH) has disappeared, indicating that the click reaction has proceeded on the surface of AuNPs.

Anion binding study

To evaluate the selectivity of ATTP-AuNPs toward various anions, the absorption spectra of ATTP-AuNPs were measured in the presence of 16 anions: Br^-, CN^-, Cl^-, ClO_4^-, F^-, HSO_4^-, $H_2PO_4^-$, HPO_4^{2-}, I^-, NO_3^-, OAc^-, OH^-, PPi, S^{2-}, $S_2O_3^{2-}$, and SCN^- (Fig. 3). Only I^- induced an obvious absorption spectral change; the color change from wine-red to purple was also observed by the naked eye (Fig. 3). Both indicate the aggregation of AuNPs. As a result of this aggregation, the absorption at 516 nm was red-shifted and the absorbance at 700 nm increased. Apparently, ATTP-AuNPs showed excellent selectivity to I^- over other anions. The HR-TEM images display the evidence of I^--induced aggregation of ATTP-AuNPs (Fig. 4). The size distribution of ATTP-

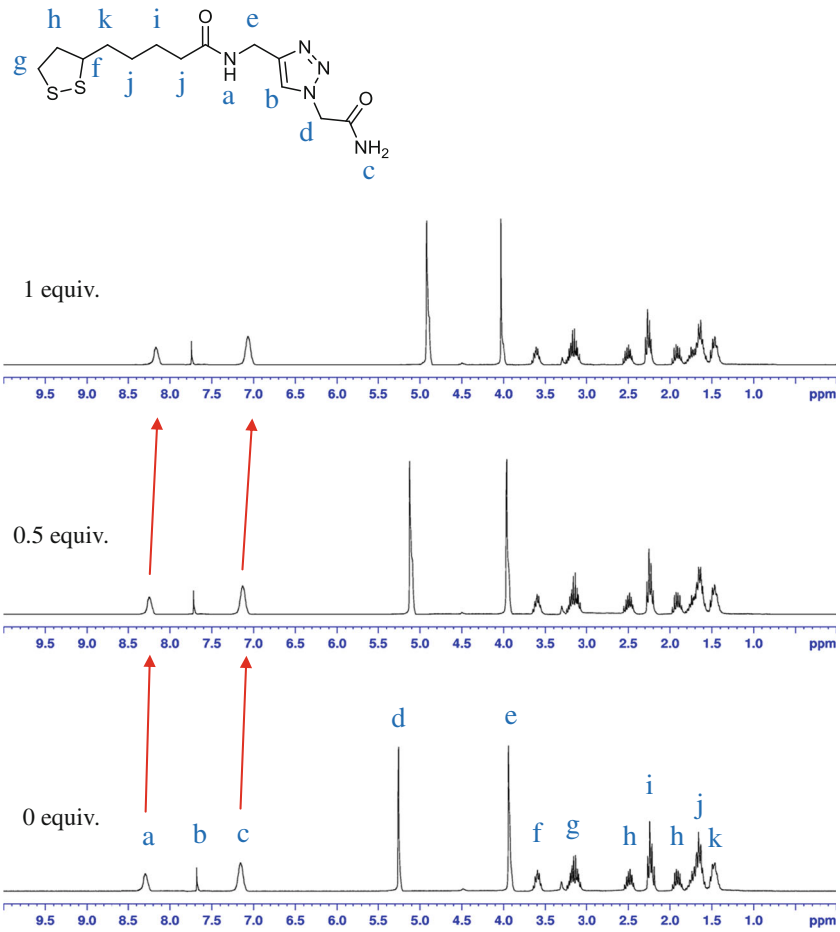

Fig. 6 ^1H NMR spectra of ATTP (30 mM) treated with various amounts of I^- in CD_3OD

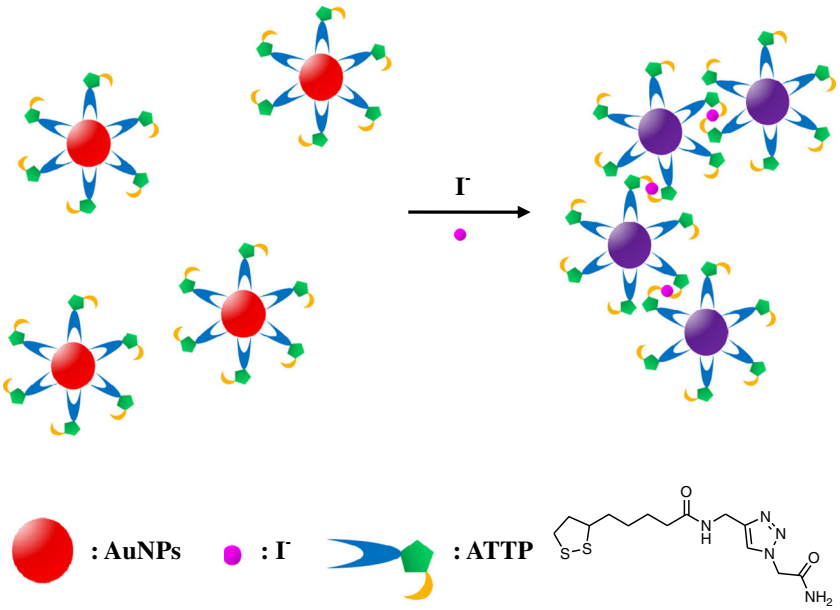

Scheme 2 Schematic depiction of the iodide-induced aggregation of ATTP-AuNPs

AuNPs was also characterized by dynamic light scattering (DLS). Figure 5 shows that the particle sizes of ATTP-AuNPs ranged from 2 nm to 10 nm, and most particle sizes fell in the range of 4.8–6.5 nm, which is similar to the size distribution observed in TEM image (Fig. 1). With addition of iodide ions, the particle sizes ranged from 20 nm to 100 nm, and most particle sizes fell in the range of 24.4–32.7 nm. This observation indicated that I^- functioned as a bridge between particles, and induced the aggregation of ATTP-AuNPs.

To gain a clearer understanding of the interaction between I^- and ATTP-AuNPs, ^{1}H NMR spectroscopy (Fig. 6) was employed. The ^{1}H NMR spectra of ATTP recorded with increasing amounts of I^- show that the amide proton signals (H_a and H_c) at δ=7.15, 8.30 ppm were shifted upfield as I^- was added. This indicates that I^- interacts with ATTP mainly through the amide protons in ATTP. Effectively, I^- functioned as a bridge between particles, and triggered the aggregation of ATTP-AuNPs (Scheme 2).

The degree of aggregation of ATTP-AuNPs depended on the concentration of I^- ions. The absorption spectra changed with the addition of various concentrations of I^- (Fig. 7). The absorbance at 516 nm decreased and that at 700 nm increased with increasing I^- concentration. A linear relationship in the plot of the absorbance at 700 nm (A_{700}) versus I^- concentration was found over the range of 0.5 to 6 μM (see the inset plot in Fig. 7). The limit of detection for I^- was found to be 15 nM (See Fig. S1 in the Supporting

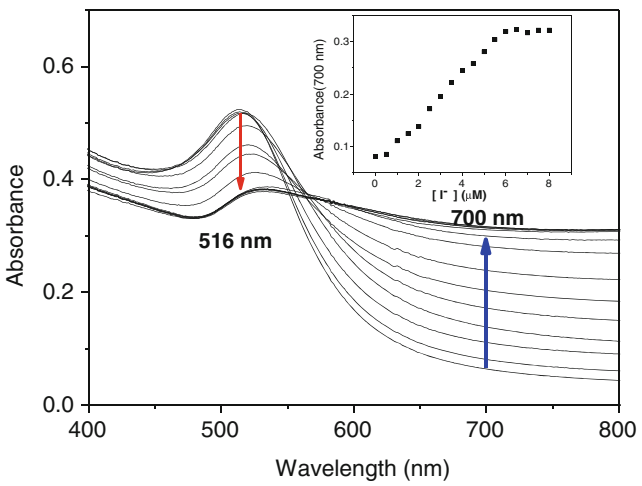

Fig. 7 Absorption spectral changes of ATTP-AuNPs in the presence of different concentrations of I^- (0–8 μM). The *inset* shows the corresponding plot of the absorbance (A_{700}) versus I^- concentration over the range of 0.5 to 6 μM

Table 1 Comparison of the proposed iodide detection method with other reported methods

Methods	Linear range (M)	Limit of detection (M)	Reference
Ion chromatography	Not reported	7.9×10^{-6}	4
Ion chromatography	5.0×10^{-9} to 5.0×10^{-7}	3.7×10^{-9}	5
Electrochemical	8.0×10^{-7} to 1.0×10^{-1}	2.5×10^{-7}	6
Electrochemical	1.0×10^{-5} to 2.0×10^{-2}	3.1×10^{-6}	7
Electrochemical	5.0×10^{-5} to 2.0×10^{-2}	1.0×10^{-5}	8
Colorimetric	3.0×10^{-5} to 1.8×10^{-4}	4.3×10^{-7}	9
Colorimetric	Not reported	5.0×10^{-6}	10
Colorimetric	Not reported	2.5×10^{-4}	11
Fluorescent	1.0×10^{-6} to 4.0×10^{-5}	Not reported	12
Fluorescent	1.0×10^{-6} to 1.3×10^{-5}	Not reported	13
Fluorescent	1.0×10^{-6} to 1.0×10^{-4}	Not reported	14
Fluorescent	1.0×10^{-6} to 1.3×10^{-5}	1.0×10^{-7}	15
Colorimetric	5.0×10^{-7} to 6.0×10^{-6}	1.5×10^{-8}	This study

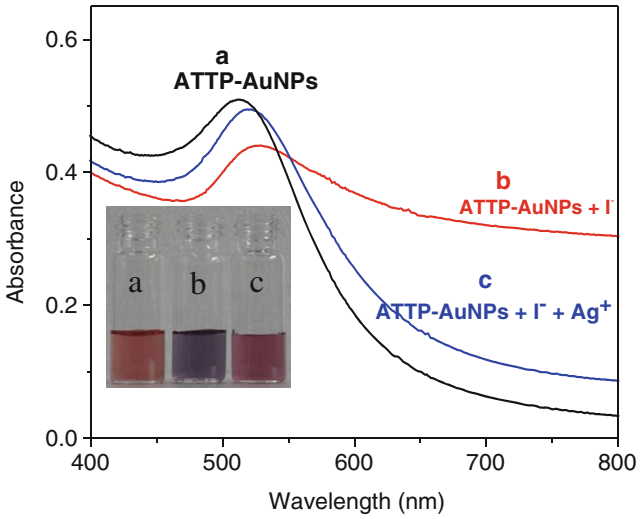

Fig. 8 Reversible binding of I^- (5 μM) with ATTP-AuNPs in the presence of Ag^+ (100 μM)

Information), which is lower than those of previously reported optical assays as shown in Table 1.

The reuse capability of ATTP-AuNPs was tested by removing I^- ions with Ag^+; this was confirmed by the consequent SPR absorption shift from 700 nm to 516 nm (Fig. 8). After removal from the solution using a centrifuge and suspension in aqueous media, the dispersed ATTP-AuNPs can be reused to detect I^-. Through this technique, the NTP-AuNP system can be used repeatedly for the detection of I^-.

Interference study

In order to study the influence of other anions on I^- binding to ATTP-AuNPs, competitive experiments were carried out in the presence of I^- with Br^-, CN^-, Cl^-, ClO_4^-, F^-, HSO_4^-, $H_2PO_4^-$, HPO_4^{2-}, I^-, NO_3^-, OAc^-, OH^-, PPi, S^{2-}, $S_2O_3^{2-}$, and SCN^- (Fig. 9). The absorbance changes caused by the

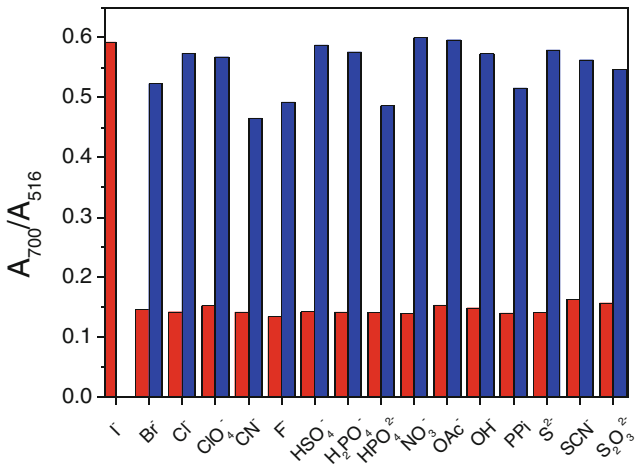

Fig. 9 Absorbance ratio (A_{700}/A_{516}) of ATTP-AuNPs in the presence of anions. *Red bars* represent the addition of single metal ion (4 μM); *blue bars* are the mixture of I^- (4 μM) with another anion (4 μM)

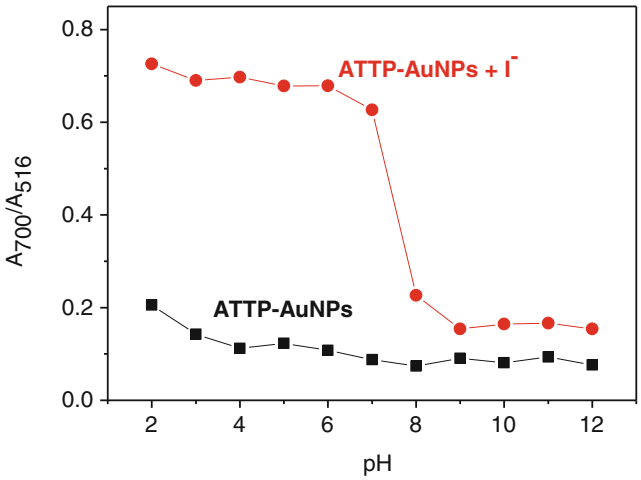

Fig. 10 Influence of pH on the absorbance ratio (A_{700}/A_{516}) of ATTP-AuNPs in the absence (■) and presence (●) of I^- (5 μM)

mixture of I^- with the other anions were similar to that caused by I^- alone. This indicates that none of the other anions interfere in the binding of ATTP-AuNPs with I^-. This observation is consistent with previous a study suggesting that I^- was the only anion which could bind to the ATTP-AuNPs.

The influence of pH on I^--induced aggregation of ATTP-AuNPs

To investigate the pH range in which ATTP-AuNPs could effectively detect I^-, a pH titration was carried out. Figure 10 shows that the absorbance ratio (A_{700}/A_{516}) of ATTP-AuNPs was constant in the pH range of 2 to 12, indicating that ATTP-AuNPs were stable in this pH range. After addition of I^-, the absorbance ratio (A_{700}/A_{516}) highly increased in the pH range of 2 to 7. At pH>7, the absorbance ratio (A_{700}/A_{516}) decreased because of the deprotonation on the amide group. Thus, the conditions at pH 2 to 7 were found to be suitable for monitoring I^- by means of the absorption change.

Analytical application in lake water

To confirm the practical application of ATTP-AuNPs, water samples from a lake located in NCTU, Hsinchu, Taiwan, were collected and spiked with different amounts of I^- standard solution. A calibration curve of the absorbance ratio

Table 2 Results of I^- detection in lake water samples

Sample	Added (μM)	Found[a] (μM)	Recovery (%)	RSD (%)	ICP-MS (μM)
Lake water	2.0	1.93	96.7	1.3	1.98
	4.0	3.92	98.1	1.6	3.97
	5.0	4.89	97.8	1.7	5.09

[a] n=3

(A_{700}/A_{516}) of ATTP-AuNPs in the presence of various concentrations of I^- was prepared (See Fig. S2 in the Supporting Information). The analytical results are shown in Table 2. The recovery was 96.7 to 98.1 %, and the values of RSD were about 1.3 to 1.7 %. The results obtained with ATTP-AuNPs were in good agreement with those obtained by ICP-MS. These results demonstrate that the designed probe was applicable for I^- detection in lake water samples.

Conclusion

In summary, new triazole-acetamide functionalized gold nanoparticles (ATTP-AuNPs) were synthesized for detecting I^-. The functionalized sensor for colorimetric sensing of I^- exhibited high selectivity in the presence of other interfering anions. This sensor offered a low-cost and fast method for monitoring I^-, and allowed detection of concentrations of as low as 15 nM. The optimal pH range for I^- detection using ATTP-AuNPs was determined to be pH 2 to 7. The sensor was applied to the analysis of I^- in lake water with recovery ranging from 96.7 to 98.1 %.

Acknowledgments We gratefully acknowledge the financial support of the National Science Council (ROC) and National Chiao Tung University.

References

1. Dai G, Levy O, Carrasco N (1996) Cloning and characterization of the thyroid iodide transporter. Nature 379:458–460
2. Rokita SE, Adler JM, McTamney PM, Watson JA (2010) Efficient use and recycling of the micronutrient iodide in mammals. Biochimie 92:1227–1235
3. Pearce EN (2012) Iodine-induced thyroid dysfunction: comment on "association between iodinated contrast media exposure and incident hyperthyroidism and hypothyroidism". Arch Intern Med 172:159–161
4. Hao FP, Haddad PR, Ruther T (2008) IC determination of halide impurities in ionic liquids. Chromatographia 67:495–498
5. Malongo TK, Patris S, Macours P, Cotton F, Nsangu J, Kauffmann J (2008) Highly sensitive determination of iodide by ion chromatography with amperometric detection at a silver-based carbon paste electrode. Talanta 76:540–547
6. Zahran EM, Hua Y, Lee S, Flood AH, Bachas LG (2011) Ion-selective electrodes based on a pyridyl-containing triazolophane: altering halide selectivity by combining dipole-promoted cooperativity with hydrogen bonding. Anal Chem 83:3455–3461
7. Chiu MH, Cheng WL, Muthuraman G, Hsu CT, Chung HH, Zen JM (2009) A disposable screen-printed silver strip sensor for single drop analysis of halide in biological samples. Biosens Bioelectron 24: 3008–3013
8. Qin X, Wang HC, Miao ZY, Wang XS, Fang YX, Chen Q, Shao XG (2011) Synthesis of silver nanowires and their applications in the electrochemical detection of halide. Talanta 84:673–678
9. Jung HJ, Singh N, Lee DY, Jang DO (2010) Single sensor for multiple analytes: chromogenic detection of I^- and fluorescent detection of Fe^{3+}. Tetrahedron Lett 51:3962–3965
10. Zhang J, Xu XW, Yang C, Yang F, Yang X (2011) Colorimetric iodide recognition and sensing by citrate-stabilized core/shell Cu@Au nanoparticles. Anal Chem 83:3911–3917
11. Kumar A, Chhatra RK, Pandey PS (2010) Synthesis of click bile acid polymers and their application in stabilization of silver nanoparticles showing iodide sensing property. Org Lett 12:24–27
12. Wang X, Zhang C, Feng L, Zhang L (2011) Screening iodide anion with selective fluorescent chemosensor. Sensors Actuators B 156: 463–466
13. Rathikrishnan KR, Indirapriyadharshini VK, Ramakrishna S, Murugan R (2011) 4,7-Diaryl indole-based fluorescent chemosensor for iodide ions. Tetrahedron 67:4025–4030
14. Lee DY, Singh N, Kim MJ, Jang DO (2011) Chromogenic and fluorescent recognition of iodide with a benzimidazole-based tripodal receptor. Org Lett 12:3024–3027
15. Zhang M, Ye BC (2012) A reversible fluorescent DNA logic gate based on graphene oxide and its application for iodide sensing. Chem Commun 48:3647–3649
16. Daniel MC, Astruc D (2004) Gold nanoparticles: assembly, supramolecular chemistry, quantum-size-related properties, and applications toward biology, catalysis, and nanotechnology. Chem Rev 104: 293–346
17. Burda C, Chen X, Narayanan R, El-Sayed MA (2005) Chemistry and properties of nanocrystals of different shapes. Chem Rev 105: 1025–1102
18. Liu D, Wang Z, Jiang X (2011) Gold nanoparticles for the colorimetric and fluorescent detection of ions and small organic molecules. Nanoscale 3:1421–1433
19. Liang G, Wang L, Zhang H, Han Z, Wu X (2012) A colorimetric probe for the rapid and selective determination of mercury(II) based on the disassembly of gold nanorods. Microchim Acta 179:345–350
20. Chansuvarn W, Imyim A (2012) Visual and colorimetric detection of mercury(II) ion using gold nanoparticles stabilized with a dithia-diaza ligand. Microchim Acta 176:57–64
21. Chen Y, Lee I, Sung Y, Wu S (2013) Triazole functionalized gold nanoparticles for colorimetric Cr^{3+} sensing. Sensors Actuators B 188: 354–359
22. Liu B, Tan H, Chen Y (2013) Visual detection of silver(I) ions by a chromogenic reaction catalyzed by gold nanoparticles. Microchim Acta 180:331–339
23. Wei S, Hsu P, Lee Y, Lin Y, Huang C (2012) Selective detection of iodide and cyanide anions using gold-nanoparticle-based fluorescent probes. ACS Appl Mater Interfaces 4:2652–2658
24. Gu J, Lin Y, Chia Y, Lin H, Huang S (2013) Colorimetric and bare-eye determination of fluoride using gold nanoparticle agglomeration probes. Microchim Acta 180:801–806
25. Wang Y, Zhu H, Yang X, Dou Y, Liu Z (2013) New colorimetric and fluorometric sensing strategy based on the anisotropic growth of histidine-mediated synthesis of gold nanoclusters for iodide-specific detection. Analyst 138:2085–2089
26. Garin D, Oukhatar F, Mahon AB, Try AC, Dubois-Dauphin M, Laferia FM, Demeunynck M, Sallanon MM, Chierici S (2011) Proflavine derivatives as fluorescent imaging agents of amyloid deposits. Bioorg Med Chem Lett 21:2203–2206
27. Dyke JM, Levita G, Morris A, Ogden JS, Dias AA, Algarra M, Santos JP, Costa ML, Rodrigues P, Barros MT (2004) A study of the thermal decomposition of 2-azidoacetamide by ultraviolet photoelectron spectroscopy and matrix-isolation infrared spectroscopy: identification of the imine intermediate $H_2NCOCHNH$. J Phys Chem A 108:5299–5307